Published in final edited form as:
Inorg Chem. 2012 October 1; 51(19): 10274–10278. doi:10.1021/ic301241s.

Site-isolated redox reactivity in a trinuclear iron complex

Emily V. Eames and **Theodore A. Betley**
Department of Chemistry and Chemical Biology, Harvard University, 12 Oxford Street, Cambridge MA 02138.

Abstract

The symmetric, high-spin triiron complex (^{Ph}L)Fe$_3$(thf)$_3$ reacts with mild chemical oxidants (e.g., Ph$_3$CX, I$_2$) to afford an asymmetric core where one iron ion bears the halide ligand (^{Ph}L)Fe$_3$X(L), and the hexadentate (^{Ph}L = MeC(CH$_2$NPh-*o*-NPh)$_3$) ligand has undergone significant rearrangement. In the absence of a suitable trapping ligand, the Cl and Br complexes form (μ-X)$_2$ bridged structures of the type [(^{Ph}L)Fe$_3$(μ-X)]$_2$. In the trinuclear complexes, the halide-bearing iron site sits in approximate trigonal bipyramidal (*tbp*) geometry formed by two (^{Ph}L) anilides and an exogenous solvent molecule. The two distal iron ions reside in distorted square-planar sites featuring a short Fe–Fe separation at 2.301 Å, whereas the distance to the *tbp* site is substantially elongated (2.6–2.7 Å). Zero-field, ^{57}Fe Mössbauer analysis reveals the diiron unit as the locus of oxidation while the *tbp* site bearing the halide ligand remains divalent. Magnetic data acquired for the series reveals the oxidized diiron unit comprises a strongly coupled S = 3/2 unit that is weakly ferromagnetically coupled to the high spin (S = 2) ferrous site, giving an overall S = 7/2 ground state for the trinuclear units.

While the collective function of polynuclear, metalloenzyme cofactors is well-described,[1] the functions of each individual metal ion within the cofactor are difficult to ascertain. Undoubtedly neighboring metal ions influence cofactor reactivity by altering substrate coordination modes and buttressing redox changes and charge distribution within the cofactor.[1a,2] We[3] and others[4] are pursuing a class of coordination complexes that feature polynuclear cores to elucidate how transition metals can cooperatively mediate redox processes and to establish what types of reactivities are possible with multiple redox reservoirs available. Utilizing a simple, hexadentate amine-based platform, we have observed facile construction of polynuclear complexes. Transamination reactions of divalent metal precursors with the amine ligand afford trinuclear metal complexes with a broad range of molecular spin states (S = 1 → 6) which vary as a function of the ligand architecture.[3a,b,g] In the iron-based complexes, use of the sterically unencumbered proton-capped ligand (^{H}L)$^{6-}$ gave rise to core delocalized redox activity,[3a] whereas use of the silylamide ligand (^{tbs}L)$^{6-}$ gave rise to atom transfer reactivity to the tri-iron core, maintaining an open-shell electronic configuration.[3b] Herein we present redox reactivity of the maximally high-spin (S = 6) triiron complex[3g] (^{Ph}L)Fe$_3$(thf)$_3$ (**1**) that gives rise to asymmetric oxidation products where coordination change occurs at an isolated ferrous ion and a distal diiron unit undergoes redox changes.

Chemical oxidation of (^{Ph}L)Fe$_3$(thf)$_3$ (^{Ph}L = MeC(CH$_2$NPh-*o*-NPh)$_3$) can be readily affected by treatment with a single equivalent of trityl-chloride (Ph$_3$CCl) in tetrahydrofuran, producing a half-equivalent of the quinoid dimer Ph$_3$C(C$_6$H$_5$)CPh$_2$ (identified by ^{1}H NMR,

Correspondence to: Theodore A. Betley.

Supporting Information Available: Experimental procedures and spectral data for **2–6**; selected crystallographic data and bond lengths for **2–6**; CIF file for **2–6**. This material is available free of charge via the internet at http://pubs.acs.org.

Scheme 1).[5] The oxidized trinuclear complex was precipitated from benzene, affording the chloride-bridged product $[(^{Ph}L)Fe_3(\mu\text{-}Cl)]_2$ (**2**) or the trinuclear product $(^{Ph}L)Fe_3Cl(py)$ (**3**) following treatment with pyridine (Scheme 1). Oxidation of **1** with trityl-bromide likewise produced both the halide-bridged products $[(^{Ph}L)Fe_3(\mu\text{-}Br)]_2$ (**4**) and solvated trinuclear $(^{Ph}L)Fe_3Br(thf)$ (**5**) from tetrahydrofuran or benzene solutions; whereas reaction of **1** with half an equivalent of iodine in tetrahydrofuran exclusively gave the trinuclear product $(^{Ph}L)Fe_3I(thf)$ (**6**). Single crystals for X-ray diffraction analysis were obtained by allowing a solution of each compound in benzene to stand at room temperature (**2, 3**, and **5**), or by cooling (−35 °C) a tetrahydrofuran solution (**4** and **6**).

The chemical compositions of the oxidized complexes **2–6** were confirmed by single crystal X-ray diffraction analysis. Representative examples of the solid-state structures for these species are provided in Figure 1. For the trinuclear complexes **3, 5**, and **6**, the molecular structure reveals three salient features: (1) two molecules of tetrahydrofuran are lost from **1**, (2) the hexa-anilide (^{Ph}L) ligand has substantially altered its binding mode, and (3) the halide ligand from chemical oxidation is bound to a single iron ion. The halide-bearing iron ion (Fe1 in Figure 1a) is nearly trigonal-monopyramidal (neglecting M–M interactions), where two ligand anilides and the pyridine form the trigonal plane and the Cl ion caps the pyramid, positioned *trans* to the diiron portion of the trinuclear core. The remaining two iron ions (Fe2, Fe3) are each bound to four ligand anilide units, forming an intermediate geometry between tetrahedral and square-planar locally at each iron, with a close Fe–Fe contact (Fe2-Fe3 2.2955(8) Å) in the axial site. The two remaining M–M contacts (Fe1-Fe2 2.7303(8) Å, Fe1-Fe3 2.6534(8) Å) are substantially elongated compared with average metal ion separation in **1** (2.491(1) Å).[3g] The trinuclear core asymmetry is maintained in the trinuclear bromide and iodide structures (see Figures S4 and 1c, respectively). The bond metrics within the (^{Ph}L) ligand *o*-phenylenediamide units are consistent with the closed-shell dianion state (see Tables S3–S7).[6]

The two hexanuclear products **2** and **4** exhibit the same structural distortions evident in the trinuclear complexes **3, 5**, and **6**. One iron ion binds the halide ligands, while the (^{Ph}L) ligand distorts to engender nearly square planar binding modes to the two remaining iron ions. The short Fe2-Fe3 contact is maintained in both of the bridged hexanuclear complexes (2.3410(5) Å in **2**, 2.3504(7) Å in **4**). While the Fe2–Fe3 ion separation is modestly elongated from the trinuclear species, the average Fe1–Fe2 and Fe1– Fe3 separations are substantially shorter (average (Å): 2.5849(5), **2**; 2.5872(7), **4**) than the distances observed in **3, 5**, and **6**. The halide bearing iron ion (Fe1 in **4** shown in Figure 1b) is more tetrahedral than the same site in the trinuclear complexes. The dihedral angle between the Br-Fe1-Br and Fe2-Fe1-Fe3 is 67.85° (68.18° in **3**), creating a twist between the two trinuclear subunits.

The one-electron oxidation of **1** results in a $[Fe^{II}{}_2Fe^{III}]$ formulation, however the locus of oxidation (the halide-bearing iron, diiron unit, or ligand residue) was not immediately apparent. . A representative zero-field ^{57}Fe Mössbauer spectrum obtained at 90 K for complex **3** is presented in Figure 2a. The spectrum reveals three distinct quadrupole doublets of equal intensity (δ, $|\Delta E_Q|$ (mm/s): 0.83, *1.67*, 33%; 0.29, *2.44*, 33%; 0.20, *2.79*, 33%). The isomer shift of the first component is consistent with a ferrous assignment and is comparable to the isomer shift found in **1** (δ, $|\Delta E_Q|$ (mm/s): 0.79, *1.25*).[3g] The two remaining quadrupole doublets are considerably shifted from **1** and feature considerably larger quadrupole splitting parameters. The significantly lowered isomer shift indicates an increase in the formal oxidation state, suggesting oxidation occurs within the diiron unit. The similarity between the isomer shifts for the two ions in the diiron unit indicate the one-electron oxidation is substantially delocalized yielding a mixed-valent diiron unit (i.e., $[Fe_2]^{5+}$). Thus, while Fe1 may bear the halide in **3**, the distal di-iron unit (Fe2-Fe3) is the

locus of oxidation, giving the formal oxidation assignment as $[Fe^{2+}(Fe_2)^{5+}]$. The spectrum for **3** is highly representative of the entire series **2–6** (see Figures S8–S11), indicating this oxidation distribution is maintained throughout the series.

The solution magnetic moments obtained for the soluble trinuclear complexes (e.g., μ_{eff} = 7.94 μ_B for **3**, 295 K C_6D_6) indicate the oxidized products maintain an open-shell configuration, although reduced from a maximally high-spin state (S = 13/2), which would exhibit a spin-only moment of 13.96 μ_B. To probe the magnetic behavior of complexes **2–6** further, variable temperature dc susceptibility data were collected in the temperature range of 5–300 K (representative data are shown for complexes **2, 3** and **5** in Figure 2b,c). In the case of **3**, $\chi_M T$ increases from a value of 6.8 cm^3 K mol^{-1} at 300 K to a maximum value of 7.4 cm^3 K mol^{-1} at 70 K (see Figure 2b). Below 50 K, the data undergo a downturn, likely the result of Zeeman and zero-field splitting. The data for trinuclear bromide **5** and iodide **6** complexes are similar (see Figures S16 and S19). The data for the hexanuclear, chloride-bridged complex **2** are nearly double that observed for trinuclear **3**. For **2**, $\chi_M T$ exhibits a maximal value of 12.8 cm^3 K mol^{-1} at 300 K, but decreases substantially below temperatures of 120 K (see Figure 2b). Variable temperature magnetization data were collected for complexes **2–6** in the temperature range of 1.8–10 K at fields of 1 to 7 T. A representative plot of reduced magnetization for **5** is shown in Figure 2c, which features a series of non-superimposable isofield curves, with the 7 T curve reaching a maximum value of M = 5.4 μ_B at 1.8 K.

Based on the Mössbauer spectra which suggest each of the oxidized trinuclear cores consist of an isolated ferrous site and a mixed-valent dinuclear unit, we modeled the data using the twospin Hamiltonian shown below (equation 1), where $\boldsymbol{S}_1$ = 2 for the ferrous ion, and $\boldsymbol{S}_2$ represents the mixed-valent diiron unit spin.

$$\hat{H} = -2J(\boldsymbol{S}_1\boldsymbol{S}_2 + \Sigma D_i \boldsymbol{S}_i^2 + g\mu_B \boldsymbol{S}\cdot\boldsymbol{B} \quad (1)$$

The spin state of the diiron $[Fe_2]^{5+}$ unit $\boldsymbol{S}_2$ will fall in the range of ½ for a maximally low-spin state, to 9/2 for a maximally high-spin state.[7] The value of $\boldsymbol{S}_2$ affects data simulations by setting the value for g, as well as and modulating the effect D_2 has on the shape of the susceptibility and reduced magnetization curves. Suitable models of the data (where g ≈ 2) were only obtained when $\boldsymbol{S}_2$ = 3/2 was used in equation 1, suggesting a total spin state of $\boldsymbol{S}$ = 7/2 for trinuclear complex which is consistent with the room temperature magnetic moments obtained for **3** ($\mu_{spin\text{-}only}$ = 7.94 μ_B for $\boldsymbol{S}$ = 7/2). The corresponding simulation using the program MAGPACK[8] that best reproduces the susceptibility and reduced magnetization data affords parameters of J = +16 cm^{-1}, D_1 = 36 cm^{-1}, D_2 = −47 cm^{-1}, and g = 2.09. The surprising decrease in D_1 as a function of halide substitution between **3** (36 cm^{-1}), **5** (14 cm^{-1}), and **6** (14 cm^{-1}) directly opposes the anticipated trend due to the larger spin-orbit coupling in the heavier halides.[9] However, the coordination environment of the halide-bearing ferrous site is altered between the complexes as a result of the halide substitution. Thus, any enhanced magnetic anisotropy imparted by the addition of the heavier halide may be offset by the change in the intra-iron spacing (see Table SI 2). The large $D2$ values for the $[Fe_2]^{5+}$ unit in **3** (−47 cm^{-1}), **5** (−95 cm^{-1}), and **6** (−110 cm^{-1}) suggest significant separation between the m_S = ±3/2 and ±1/2 levels. Though these values are large, they are in accord with other dinuclear species featuring a large degree of metal–metal orbital overlap. most notably the $[Ru_2]^{5+}$ and $[Ru_2]^{6+}$ complexes where D up to 70 cm^{-1} and 260 cm^{-1}, respectively, have been observed.[10]

Modifying the Hamiltonian spin expression to account for an additional exchange interaction J_2 (between the two trinuclear subunits mediated through the bridging halides in**2**), we modeled the data for **2** using the following expression (equation 2):

$$\hat{H} = -2J_1(\boldsymbol{S}_{1_a}\boldsymbol{S}_{2_a} + \boldsymbol{S}_{1_b}\boldsymbol{S}_{2_b}) - 2J_2(\boldsymbol{S}_{1_a}\boldsymbol{S}_{1_b}) + \Sigma D_i \boldsymbol{S}_i^2 + g\mu_B \boldsymbol{S}\cdot\boldsymbol{B} \quad (2)$$

The simulation that best reproduces the data for **2** affords parameters of $J_1 = +15\ cm^{-1}$, $J_2 = -1.5\ cm^{-1}$, $D_1 = 40\ cm^{-1}$, $D_2 = -120\ cm^{-1}$, and $g = 2.17$; and for **4**: $J_1 = +20\ cm^{-1}$, $J_2 = -1.25\ cm^{-1}$, $D_1 = 43\ cm^{-1}$, $D_2 = -95\ cm^{-1}$, and $g = 2.28$. The weak antiferromagnetic coupling between the trinuclear subunits leads to the $S = 0$ ground state for the hexanuclear, halide-bridged complexes **2** and **4** (see Figures S13, S17), contributing to the downturn in the susceptibility data at lower temperatures. At higher temperatures, the susceptibility data is nearly twice the values observed for trinuclear **3**, consistent with two spin-independent trinuclear subunits in **2**. This assessment is corroborated by the reduced magnetization data for **2** and **4** (see Figures S12, S14).

The electronic structure within the trinuclear cores deviates from our previous work, wherein redox was symmetricallydistributed within the polynuclear core.[3a,c] In previous examples, bonding metrics within the polynuclear core are affected by direct orbital-orbital interactions between adjacent metal sites. Upon oxidation of the low-spin congener $(^{H}L)Fe_3(PMe_3)_3$, the contraction observed within the trinuclear core is attributed to depopulation of a nominally antibonding interaction.[3a] In the present case, chemical oxidation of **1** leads to increased metal-metal interaction within the dinuclear site of oxidation, while simultaneously attenuating the interaction with the lone ferrous site. The iron-anilide (Fe-N 2.078(3) Å) and iron-halide bond metrics for Fe1 in **3** are consistent with a high-spin ferrous assignment. The close ironiron separation in the oxidized diiron unit $[Fe_2]^{5+}$ suggests significant M–M orbital overlap. The diiron unit is approximated as two edge-sharing square planar ions giving rise to the direct orbital interactions as illustrated in Scheme 2. Population of the eleven valence electrons into this manifold will not fill the three highest lying σ* orbitals, which represent $(Fe–N)_{\sigma}^{*}$ and $(Fe–Fe)_{\sigma}^{*}$ interactions, the latter arising from the antibonding combination of the Fe d_{z^2}. Consistent with this model, the average Fe–N distance in **3** (1.936(5) Å) are considerably shorter than high-spin **1** (2.176(5) Å) where these orbital interactions are populated.

The above analysis, based on crystallographic, magnetic, and Mössbauer spectral data suggest a new mechanism by which redox is mediated within polynuclear complexes. In the low-spin regime, oxidation is delocalized throughout the trinuclear core. Mössbauer data obtained upon atom-transfer to the high-spin $(^{tbs}L)Fe_3(thf)$ complex suggests the two-electron oxidation incurred upon nitride formation is core-delocalized.[3b] However, the foregoing data describing the chemical oxidation of high-spin $(^{Ph}L)Fe_3(thf)_3$ demonstrate that oxidation leads to a trapped valency within a diiron unit, separate from the apparent site of halide capture, with concomitant rearrangement of the trinucleating ligand. These observations are analogous to previously reported redox-induced electron transfer reactivity exhibited by redoxactive ligands. Typically such ligand reorganization presents a large energy barrier, but the maximally high-spin formulation of the all-ferrous precursor creates an inherently labile system. Furthermore, the elucidation of this unusual mode of cooperative redox reactivity demonstrates the potential of polynuclear complexes to provide insight into how redox processes may occur within polynuclear metallocofactors in nature.

Supplementary Material

Refer to Web version on PubMed Central for supplementary material.

Acknowledgments

The authors thank Harvard University and NIH (GM 098395) for financial support, Prof. R. H. Holm for the generous use of his Mössbauer spectrometer, and the Harvard University Center for the Environment for funding (EVE).

REFERENCES

1. Nitrogenase: Burgess BK, Lowe DJ. Chem. Rev. 1996; 96:2983–3012. [PubMed: 11848849] Dos Santos PC, Igarashi RY, Lee HI, Hoffman BM, Seefeldt LC, Dean DR. Acc. Chem. Res. 2005; 38:208–214. [PubMed: 15766240] Hoffman BM, Dean DR, Seefeldt LC. Acc. Chem. Res. 2009; 42:609–619. [PubMed: 19267458] Photosystem II: Nugent J. Biochim. Biophys. Acta. 2001; 1503:1. [PubMed: 11115619] Ferreira KN, Iverson TM, Maghlaoui K, Barber J, Iwata S. Science. 2004; 303:1831. [PubMed: 14764885] Iwata S, Barber J. Curr. Opin. Struct. Biol. 2004; 14:447. [PubMed: 15313239] N_2O reductase: Brown K, Djinovic-Carugo K, Haltia T, Cabrito I, Saraste M, Moura JJG, Moura I, Tegoni M, Cambillau C. J. Biol. Chem. 2000; 275:41133. [PubMed: 11024061] Brown K, Tegoni M, Prudêncio M, Pereira AS, Besson S, Moura JJ, Moura I, Cambillau C. Nat. Struct. Biol. 2000; 7:191. [PubMed: 10700275] Chen P, George SD, Cabrito I, Antholine WE, Moura JG, Moura I, Hedman B, Hodgson KO, Solomon EI. J. Am. Chem. Soc. 2002; 124:744. [PubMed: 11817937]
2. (a) Fontecilla-Camps JC. J. Biol. Inorg. Chem. 1996; 96:3031.(b) Siegbahn PEM. Inorg. Chem. 2000; 39:2923. [PubMed: 11232834] (c) Huniar U, Ahlrichs R, Coucouvanis D. J. Am. Chem. Soc. 2004; 126:2588. [PubMed: 14982469]
3. (a) Zhao Q, Betley TA. Angew. Chem. Int. Ed. . 2011; 50:709–712.(b) Powers TM, Fout AR, Zheng SL, Betley TA. J. Am. Chem. Soc. 2011; 133:3336. [PubMed: 21332160] (c) Zhao Q, Harris TD, Betley TA. J. Am. Chem. Soc. 2011; 133:8293. [PubMed: 21561083] (d) Harris TD, Zhao Q, Hernández Sánchez R, Betley TA. Chem. Commun. 2011; 47:6344.(e) Harris TD, Betley TA. J. Am. Chem. Soc. 2011; 133:13852. [PubMed: 21815671] (f) Fout AR, Zhao Q, Xiao DJ, Betley TA. J. Am. Chem. Soc. 2011; 133:16750. [PubMed: 21942370] (g) Eames EV, Harris TD, Betley TA. Chem. Sci. 2012; 3:407.
4. (a) Adams RD. J. Organometallic Chem. 2000; 600:1–6.(b) Suzuki H. Eur. J. Inorg. Chem. 2002:1009–1023.(c) Dyson PJ. Coord. Chem. Rev. 2004; 248:2443–2458.(d) Pap JS, DeBeer George S, Berry JF. Angew. Chem. Int. Ed. 2008; 47:10102–10105.
5. Gomberg M. J. Am. Chem. Soc. 1900; 22:757.
6. (a) Balch AL, Holm RH. J. Am. Chem. Soc. 1966; 88:5201.(b) Warren LF. Inorg. Chem. 1977; 16:2814.(c) Chaudhuri P, Verani CN, Bill E, Bothe E, Weyhermüller T, Wieghardt K. J. Am. Chem. Soc. 2001; 123:2213. [PubMed: 11456867] (d) Anillo A, Diaz MR, Garcia-Granda S, Obeso-Rosete R, Galindo A, Ienco A, Mealli C. Organometallics. 2004; 23:471.(d) Bill E, Bothe E, Chaudhuri P, Chlopek K, Herebian K, Kokatam S, Ray K, Weyhermüller T, Neese F, Wieghardt K. Chem. Eur. J. 2005; 11:204. [PubMed: 15549762] (e) Chlopek K, Bill E, Weyhermüller T, Wieghardt K. Inorg. Chem. 2005; 44:7087. [PubMed: 16180871]
7. (a) Drüeke S, Chaudhuri P, Pohl K, Wieghardt K, Ding XQ, Bill E, Sawaryn A, Trautwein AX, Winkler H, Gurman SJ. Chem. Commun. 1989:59.(b) Ding XQ, Bominaar EL, Bill E, Winkler H, Trautwein AX, Drüeke S, Chaudhuri P, Wieghardt K. J. Chem. Phys. 1990; 92:178.(c) Dutta SK, Ensling J, Werner R, Flörke U, Haase W, Gütlich P, Nag K. Angew. Chem. Int. Ed. 1997; 36:152. (d) LeCloux DD, Davydov R, Lippard SJ. J. Am. Chem. Soc. 1998; 120:6810.(e) Lee D, Krebs C, Huynh BH, Hendrich M, Lippard SJ. J. Am. Chem. Soc. 2000; 122:5000.(f) Hazra S, Sasmal S, Fleck M, Grandjean F, Sougrati MT, Ghosh M, Harris TD, Bonville P, Long GJ, Mohanta S. J. Chem. Phys. 2011; 134:174507. [PubMed: 21548699]
8. Borrás-Almenar JJ, Clemente-Juan JM, Coronado E, Tsukerblat BS. J. Comput. Chem. 2001; 22:985.
9. Karunadasa HI, Arquero KD, Berben LA, Long JR. Inorg. Chem. 2010; 49:4738. [PubMed: 20443564]
10. (a) Bennett MJ, Caulton KG, Cotton FA. Inorg. Chem. 1969; 8:1.(b) Angaridis P, Cotton FA, Murillo CA, Villagran D, Wang X. J. Am. Chem. Soc. 2005; 127:5008. [PubMed: 15810821] (c) Barral MC, Gallo T, Herrero S, Jimenez-Aparicio R, Torres MR, Urbanos FA. Inorg. Chem. 2006;

45:3639. [PubMed: 16634596] (d) Barral MC, Gallo T, Herrero S, Jimenez-Aparicio R, Torres MR, Urbanos FA. Chem.-Eur. J. 2007; 13:10088. [PubMed: 17907129] (e) Chiarella GM, Cotton FA, Murillo CA, Young MD, Zhao Q. Inorg. Chem. 2010; 49:3051. [PubMed: 20151686]

11. (a) Min KS, DiPasquale AG, Golen JA, Rheingold AL, Miller JS. J. Am. Chem. Soc. 2007; 129:2360. [PubMed: 17269771] (b) Min KS, DiPasquale AG, Rheingold AL, White HS, Miller JS. J. Am. Chem. Soc. 2009; 131:6229. [PubMed: 19358538]

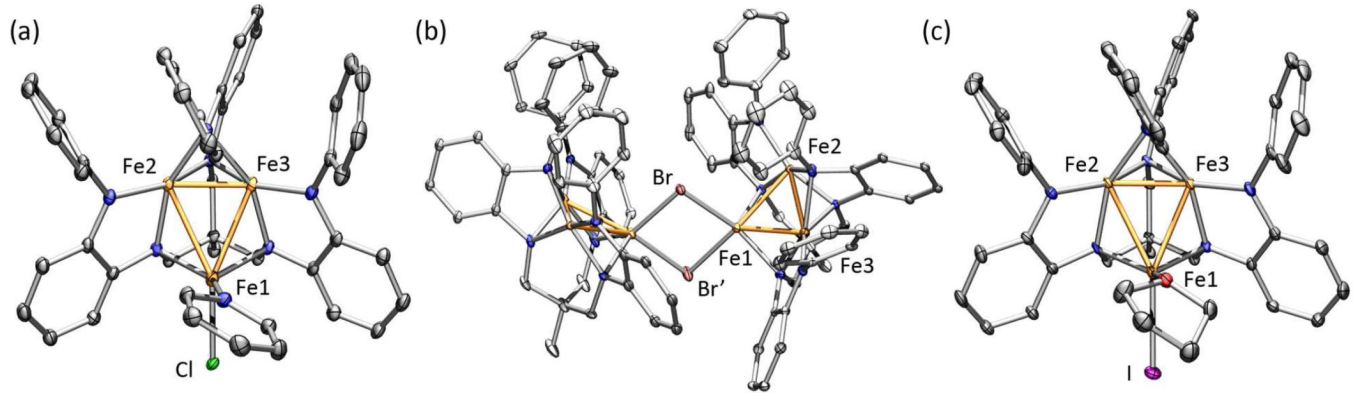

Figure 1.

Solid-state structures for (a) (^{Ph}L)Fe$_3$Cl(py) (**3**), (b) [(^{Ph}L)Fe$_3$(μ-Br)]$_2$ (**4**), and (c) (^{Ph}L)Fe$_3$I(thf) (**6**) with the thermal ellipsoids set at the 50% probability level (hydrogen atoms, and solvent molecules omitted for clarity; Fe orange, C black, H white, N blue, O red, Cl green, Br brown, I magenta). Bond lengths (Å) for **3**: Fe1-Fe2, 2.7303(8); Fe1-Fe3, 2.6534(8); Fe2-Fe3, 2.2955(8); Fe1-Cl, 2.3333(11); Fe1-N$_{py}$, 2.066(3); for **4**: Fe1-Fe2, 2.5871(7); Fe1-Fe3, 2.5873(7); Fe2-Fe3, 2.3504(7); Fe1-Br1, 2.5715(6), Fe1-Br2, 2.4670(6); Fe1-Fe1, 3.5810(11); for **6**: Fe1-Fe2, 2.6026(10); Fe1-Fe3, 2.6971(11); Fe2-Fe3, 2.3079(10); Fe1-I, 2.6695(9); Fe1-O, 2.024(4).

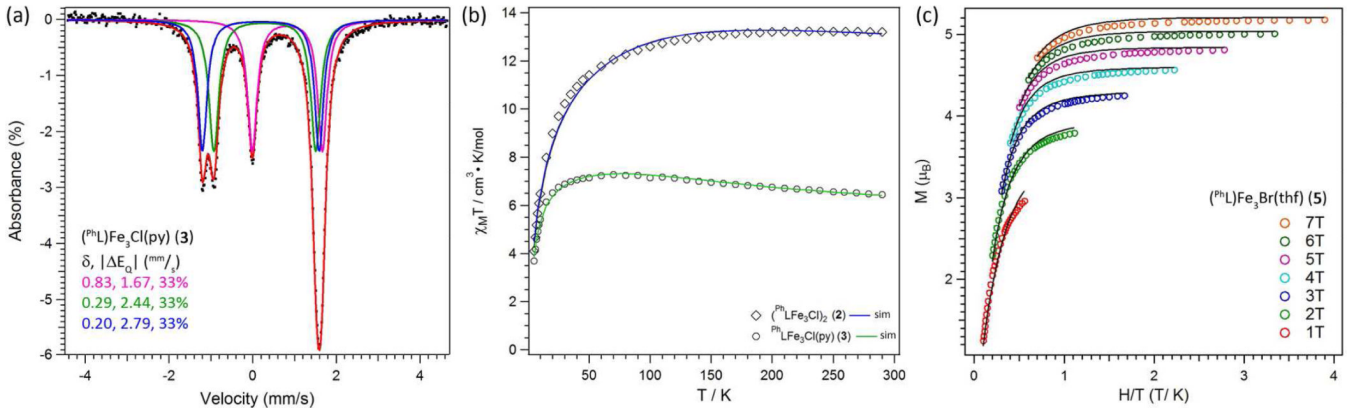

Figure 2.

(a) Zero-field ^{57}Fe Mössbauer spectrum obtained at 90 K and spectral fits (δ, $|\Delta E_Q|$ (mm/s)) for **3** (component 1 (magenta): 0.83, *1.67*, 33%; component 2 (green): 0.29, *2.44*, 33%; component 3 (blue): 0.20, 2.79, 33%). (b) Variable-temperature magnetic susceptibility data for **2** (diamonds) and **3** (circles) collected in an applied dc field of 0.1 T. Solid lines represent simulations to the data as described in the text. (c) Plot of reduced magnetization for **5** between 1.8 and 10 K at applied fields of 1–7 T.

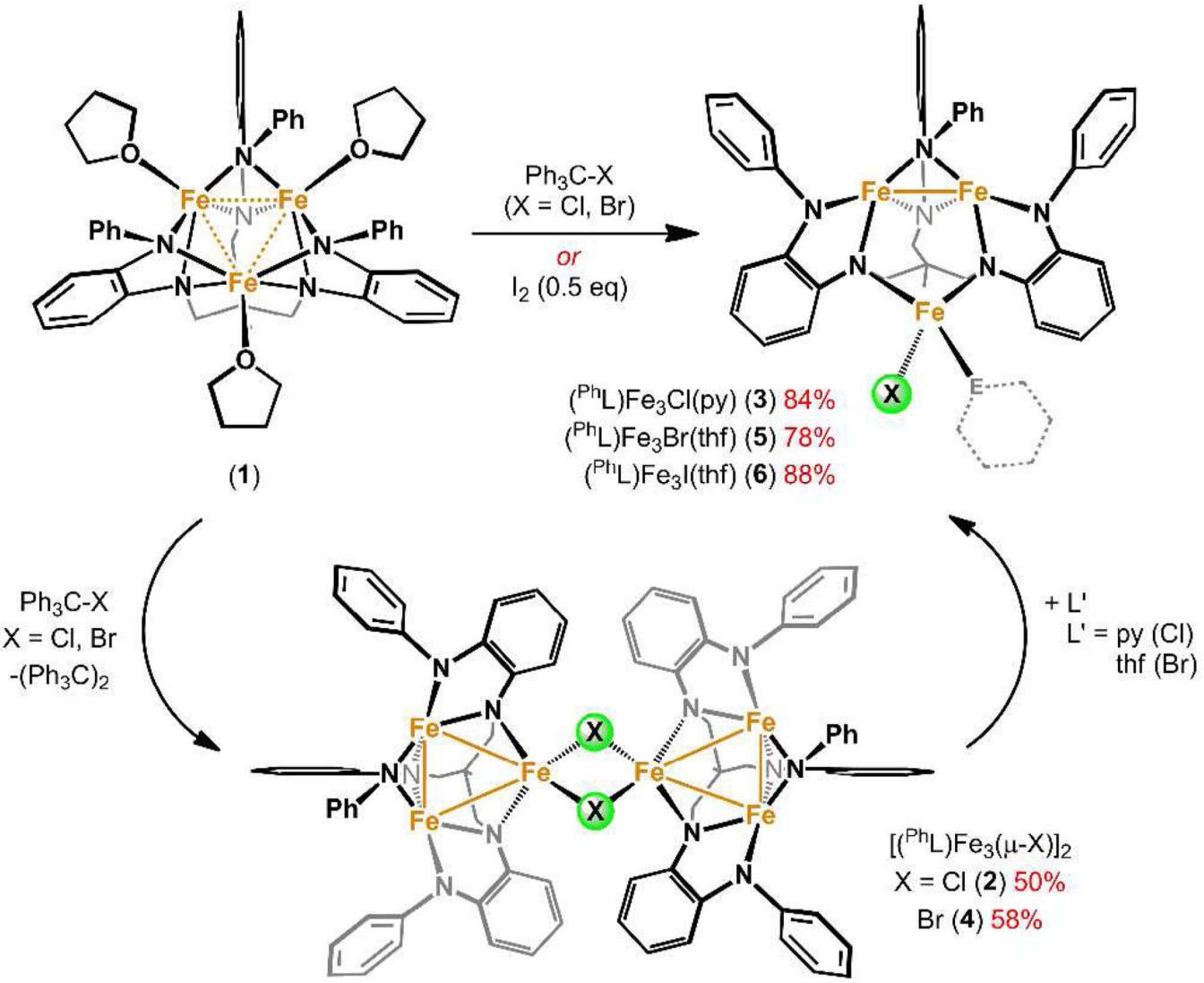

Scheme 1.

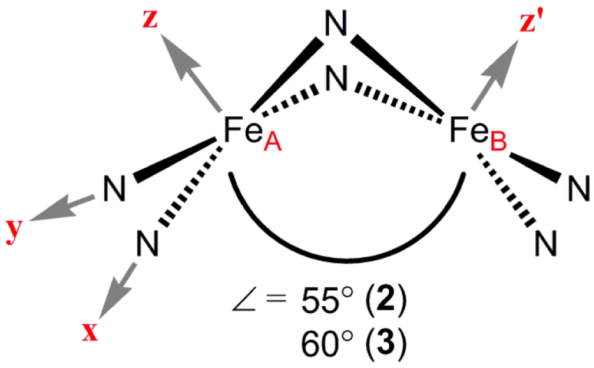

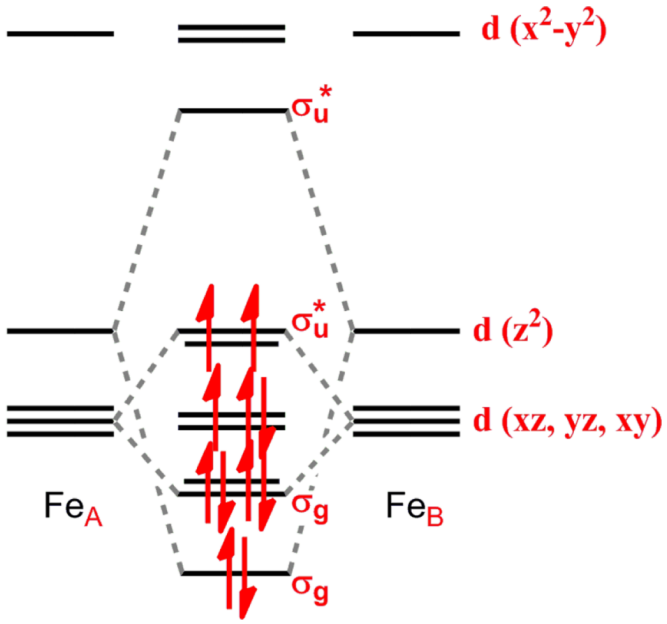

Scheme 2.